Chem. Senses 27: 789–801, 2002

Oscillatory Current Responses of Olfactory Receptor Neurons to Odorants and Computer Simulation Based on a Cyclic AMP Transduction Model

Noriyo Suzuki, Masakazu Takahata and Koji Sato[1]

Animal Behavior and Intelligence, Division of Biological Sciences, Graduate School of Science, Hokkaido University, Sapporo 060-0810, Japan

[1]Present address: Department of Fisheries, Wildlife and Conservation Biology, University of Minnesota, 200 Hodson Hall, 1980 Folwell Avenue, St Paul, MN 55108, USA

Correspondence to be sent to: Dr Noriyo Suzuki, Animal Behavior and Intelligence, Division of Biological Sciences, Graduate School of Science, Hokkaido University, Sapporo 060-0810, Japan. e-mail: suzuki@sci.hokudai.ac.jp

Abstract

Neural oscillatory activities triggered by odorant stimulation have been often reported at various levels of olfactory nervous systems in vertebrates. To elucidate the origin of neural oscillations, we studied first the oscillatory properties of current responses of isolated olfactory receptor neurons (ORNs) of the rainbow trout to amino acid odorants, using a whole-cell voltage-clamp technique and found that the damped current oscillations were intrinsic in both ciliated and microvillous ORNs and occurred when ORNs were stimulated by odorants at high intensities. Continuous wavelet analysis using the Gabor function revealed that the dominant frequency of oscillations was 1.89 ± 0.50 Hz (mean ± SD, $n = 92$). There was no significant difference in oscillation frequency between the two types of ORNs and between different perfusion conditions with standard and Na^+-free (choline) Ringer's solutions, but there was a slight difference in oscillation frequency between different holding potential conditions of negative and positive potentials. We then performed a computer simulation of the current responses with a cAMP olfactory transduction model. The model was based on the assumption that the current responses of ORNs were linearly related to the sum of concentrations of active cyclic-nucleotide-gated channels and Ca^{2+}-activated Cl^- channels, and was expressed by 12 differential equations with 44 different parameters. The simulation revealed that the oscillations of current responses of ORNs were mainly due to the oscillatory properties of intracellular cAMP and Ca^{2+} concentrations. The necessary reaction component for the oscillations in the transduction model was direct inhibition of adenylate cyclase activity by Ca^{2+}. High Ca^{2+} efflux by the Na^+–Ca^{2+} exchanger and cAMP-phosphodiesterase activity were most influential on the oscillations. The simulation completely represented the characteristics of current responses of ORNs: odorant-intensity-dependent response, intensity-dependent latency and adaptation. Thus, the simulation is generally applicable to current and voltage responses of ORNs equipped with cAMP olfactory transduction pathway in other vertebrate species. The simulation programs for Macintosh (cAMP 9.2.7 and 9.2.8 for MacOS 8.1 or later) and cAMP JAVA applet versions based on cAMP 9.2.8 have been published on the world wide web (http://bio2.sci.hokudai.ac.jp/bio/chinou1/noriyo_home.html).

Introduction

Since the pioneering work on olfactory physiology by Adrian (Adrian, 1955), neural oscillatory activities triggered by odorant stimulation have often been reported at various levels of olfactory nervous systems in a wide variety of vertebrates: fish (Sutterlin and Sutterlin, 1971; Tucker and Suzuki, 1972); amphibians (Ottoson, 1956, 1959a; Takagi and Shibuya, 1960a,b, 1961; Hamilton and Kauer, 1989); reptiles (Tucker, 1975a,b); birds (Shibuya and Tucker, 1967); and mammals (Adrian, 1956; Ottoson, 1959b; Mathews, 1972).

The oscillatory activities in the peripheral and higher olfactory nervous system have recently been restudied in order to determine their role in odorant information coding. The oscillations of electro-olfactograms (EOGs) occur in their decay phases in response to different odorants and their dominant frequencies are 28 Hz in the channel catfish (Parker *et al*., 1999) and 16 Hz in the toad (Nakazawa *et al*., 2000). It has been shown (Parker *et al*., 2000) that the dominant frequency of oscillations of summated impulse responses of small populations of olfactory receptor neurons (ORNs) to amino acid odorants was 13–37 Hz and that the oscillations were triggered and enhanced by trisodium citrate with its action of Ca^{2+} chelation from the surface of the olfactory epithelium. Optical recordings of odorant

responses from different loci in the turtle olfactory bulb have shown that there are three different oscillations with different frequencies in the olfactory bulb (Lam *et al*., 2000). Simultaneous recordings of EOGs or summated impulse responses of small populations of ORNs (peripheral waves—PWs) and summated impulse responses of small populations of neurons at different bulbar loci (local field potentials—LFPs) to volatile odorants in the salamander (Dorries and Kauer, 2000) and amino acid odorants in the channel catfish (Nikonov and Caprio, 2001; Nikonov *et al*., 2002) have shown that the PWs and the LFPs are cross-correlated; the frequency and magnitude of the LFPs increased with PWs and their oscillations are phase-locked. These studies suggest that the oscillations of both levels share a common source and are modulated together and that their common source might be the oscillatory properties of individual ORNs in the olfactory epithelium.

The characteristic frequency ranges of neural oscillations in different nervous systems are basically determined by two types of features; one is patterns of connectivity between neurons and the dynamic properties of the intervening synapses and the other is the network rhythmicity that arises via the coupling of oscillatory subunits, each of which possesses an intrinsically determined frequency preference, although these two features are not mutually exclusive since network connectivity could reinforce the patterns of excitation produced by coupled oscillators (Hutcheon and Yarom, 2000). In the olfactory nervous system, such independent and intrinsic oscillatory activities have actually been observed in isolated ORNs (Frings and Lindemann, 1988) and in the olfactory bulb slice preparation (Desmaisons *et al*., 1999). Reisert and Matthews (Reisert and Matthews, 1997, 2001a,b) reported that the oscillation frequency of isolated ORNs in response to a prolonged odorant stimulation of 30 s was 0.083–0.28 Hz in the frog and 0.42–2.70 Hz in the mouse. They suggested that the oscillations might be due to the Na^+–Ca^{2+} ion exchanger (NCX) mechanisms in the membrane of ORNs. We also have noticed the oscillations superimposed on current responses of isolated ORNs from the rainbow trout in our previous patch-clamp studies (Sato and Suzuki, 2000, 2001).

In the present work, we studied the oscillatory properties of current responses of isolated ORNs from the rainbow trout and performed a computer simulation of current responses of ORNs based on a cAMP transduction model in order to elucidate the origin of oscillations in ORNs. The simulation studies revealed that the oscillations of current responses of ORNs are mainly due to the oscillatory properties of intracellular cAMP and Ca^{2+} concentrations and that the necessary reaction component for the oscillations in the transduction model is the direct inhibition of adenylate cyclase (AC) activity by Ca^{2+}. High Ca^{2+} effluxes by NCX and cAMP-phosphodiesterase (cAMP-PDE) activity were most influential on the oscillations. The simulation completely represented the characteristics of current responses of ORNs: odorant-intensity-dependent response, intensity-dependent latency and adaptation.

Materials and methods

Whole-cell current recordings of isolated ORNs from rainbow trout

The ORNs of rainbow trout (fork length, 17–20 cm; weight, 60–90 g) obtained from a local fishery were isolated for whole-cell patch-clamp recordings. Cell isolation by the Ca^{2+}-free solution method and whole-cell voltage-clamp recordings using a pressure ejection stimulation system were performed as described previously (Sato and Suzuki, 2000, 2001). Briefly, both types of ORNs—ciliated (cORNs) and microvillous (mORNs)—were isolated and stimulated focally at their cilia or microvilli with a quadruple amino acid mixture (1.0 or 10 mM: L-Glu, L-Arg, L-Ala and L-Nva) in the perfusion of standard Ringer's solution (in mM: NaCl, 100; KCl, 3; $CaCl_2$, 2; $MgCl_2$, 1; D-glucose, 10; HEPES, 5; NaOH, 2.2; pH 7.4) or Na^+-free (choline) Ringer's solution (in mM: choline-Cl, 100; KCl, 3; $CaCl_2$, 2; $MgCl_2$, 1; D-glucose, 10; HEPES, 5; NaOH, 2.2; pH 7.4) in order to record Ca^{2+}-activated Cl^- ion channel current responses. The calibration of the waveforms of ejected odorant pulses, examined by measuring liquid junction currents and voltages, confirmed that there were no measurable bumps superimposed on the odorant pulses. The recording pipette was filled with K^+-internal solution (in mM: KCl, 93; EGTA-2K, 5; HEPES, 5; ATP-2Na, 1.0; GTP-Na, 0.1; KOH, 2.26; pH 7.4] and its resistance was 8–12 MΩ. The recording pipette was connected via a silver–silver-chloride (Ag–AgCl) wire to the headstage of a patch-clamp amplifier (CEZ-2200; Nihon Kohden, Tokyo). The reference electrode was an Ag–AgCl plate immersed in the bath solution. Current signals were low-pass filtered at 3 kHz and stored on magnetic tape using a PCM data recorder (DC-13 kHz bandwidth; PCM-501ES; Sony, Tokyo) for later off-line analysis.

Analysis of oscillatory properties of current responses

Current response data for a period of 5 or 15 s were first low-pass filtered at 40 Hz (4 dB/oct, Butterworth) and digitized at 200 Hz sampling speed using PowerLab Chart 3.6.8 (AD Instruments, Mountain View, CA) on a Power Macintosh computer and the data for each record were transformed into the file format for Igor Pro 4.0 (WaveMetrics, Lake Oswego, OR). The data files were then displayed as Igor Pro graphs and their decay phase was fitted by a double exponential function curve. The data of the fitted function curve were subtracted from the decay phase data of the record and the residue data for the decay phase were obtained for each record and transformed into a text file format. The text files were then subjected to a continuous wavelet analysis using a JAVA software MEM—maximum entropy method (Ishikawa, 2000)—with

the eighth-order Gabor function (Mallat, 1999). The power density of the frequency for each record was analyzed at eight levels, each of which was divided into four divisions, in the frequency range between 0.19 and 32.02 Hz. The analyzed data for each record were displayed on a computer screen as an 8 bit grayscale diagram with axes of frequency on ordinate and time on abscissa. The text files of the residue data of records were also subjected to the calculation of mean of root mean square (RMS) for the evaluation of signal fluctuation by PowerLab Chart 4.1.1. The statistical evaluation of frequency analysis data was performed using StatView 4.5 (SAS Institute, Cary, NC).

Development of simulation programs

Simulation programs of the current responses for a Power Macintosh computer were developed with REALbasic 3.5J (REAL Software, Austin, TX) based on a cAMP transduction pathway model for the current responses (Figure 3). The model was constructed on the basis of cAMP second messenger system models for neurons at different levels of the nervous system (Cooper *et al*., 1995; Bhalla and Iyengar, 1999), using some of the parameter values in the references cited in review articles (Zufall *et al*., 1994; Nakamura, 2000) and empirically determined parameter values. Although most functional molecules in the olfactory transduction pathway are thought to be concentrated in the membranes of olfactory cilia or microvilli, it was assumed in the present model that these functional molecules are evenly distributed in the cell (Bhalla and Iyengar, 1999). The unit conductances of cyclic-nucleotide-gated (CNG) ion channels and Ca^{2+}-activated Cl^- (CAC) ion channels were also ignored, so that the whole-cell current responses were assumed to be linearly related to the sum of concentrations of active CNG and CAC channels for an ORN. In addition, IP_3-involved reaction processes and CO/cGMP-involved processes that have been proposed to exist in the olfactory transduction pathways in fishes (Restrepo *et al*., 1990, 1993; Lo *et al*., 1993; Cadiou *et al*., 2000) and in mammals and amphibians (Schild *et al*., 1995; Lischka *et al*., 1999; Zufall and Leinders-Zufall, 1997) were excluded to avoid complicating the simulation procedure. Thus, the reaction processes in the model were expressed by 12 differential equations with 44 different parameters (see Appendix). The simulation programs for Macintosh (cAMP 9.2.7 and 9.2.8 for MacOS 8.1 or later) and the cAMP JAVA applet versions based on cAMP 9.2.8 (http://bio2.sci.hokudai.ac.jp/bio/chinou1/noriyo_home.html) calculate numerical solutions using the Euler integration method or the 4th-order Runge–Kutta integration method (Gershenfeld, 1999; Schutter, 2001) on a fixed integration time step, usually 0.001 s or shorter and display the solutions for 12 different functions expressed as the concentration in μM on the ordinate versus the time in seconds on the abscissa. The time scale of the abscissa is changeable up to 10 s for cAMP 9.2.7 and 100 s for cAMP 9.2.8. The polarity and scale of the ordinate are changeable for the numerical solution curves to represent similarly as actual inward current responses, especially for the sum of concentrations of active CNG and CAC channels. The programs also export the solution files as reversible row text tables for Igor Pro, from which the three-dimensional graphs were obtained using its surface plot option.

All graphs obtained by the various software packages in the present study were further processed for presentation using Canvas 6 graphics software (Deneba, Miami, FL).

Results

Oscillations of whole-cell inward current responses

Figure 1A illustrates typical whole-cell current responses of a cORN to the amino acid mixture puff with a 25 ms duration at a holding potential of –60 mV. The amplitude of inward current response increased with increased odorant intensity, as the odorant intensity was shown to relate linearly to the ejection pressure (Sato and Suzuki, 2000). Since the responses were all phasic, with a fast rise and slower exponential decay, the decay phases of responses were fitted by different double exponential function curves. The fitted function curve data were subtracted from the decay phase data of the record and the residue data for the decay phase were obtained. The corresponding residue noises to the original responses in Figure 1A are shown in Figure 1B. The signal fluctuation measured by the mean of RMS for these residue noises increased with increased odorant intensity and the residue noises became more oscillatory with increases of signal fluctuation, i.e. the oscillations occurred in high odorant intensity ranges. The positive correlation between the current response peak and the signal fluctuation of residual noises (r = 0.78, n = 23 records from four cORNs) also indicated that the oscillations appeared in the responses of ORNs when stimulated by odorants in high intensity. The residue noise records were then subjected to wavelet analysis and displayed as power density diagrams for frequency versus time relation, as shown in Figure 1C.

Figure 2A shows whole-cell current responses of an mORN to the amino acid mixture with different prolonged stimulus durations (1, 3 and 5 s; 1 kgf/cm^2) at a holding potential of –60 mV and the fitted double exponential function curves to their decay phases. The residue noise was subjected to wavelet analysis to show its dominant frequency (Figure 2B).

Oscillation frequency of whole-cell current responses

Table 1 summarizes the oscillation frequencies of whole-cell current responses determined by wavelet analysis under different recording conditions. The mean of theoscillation frequencies of current response records from 41 ORNs (31 cORNs and 10 mORNs) was 1.89 ± 0.50 Hz (mean ± SD, n = 92, range 0.98–3.51). There was no statistical difference

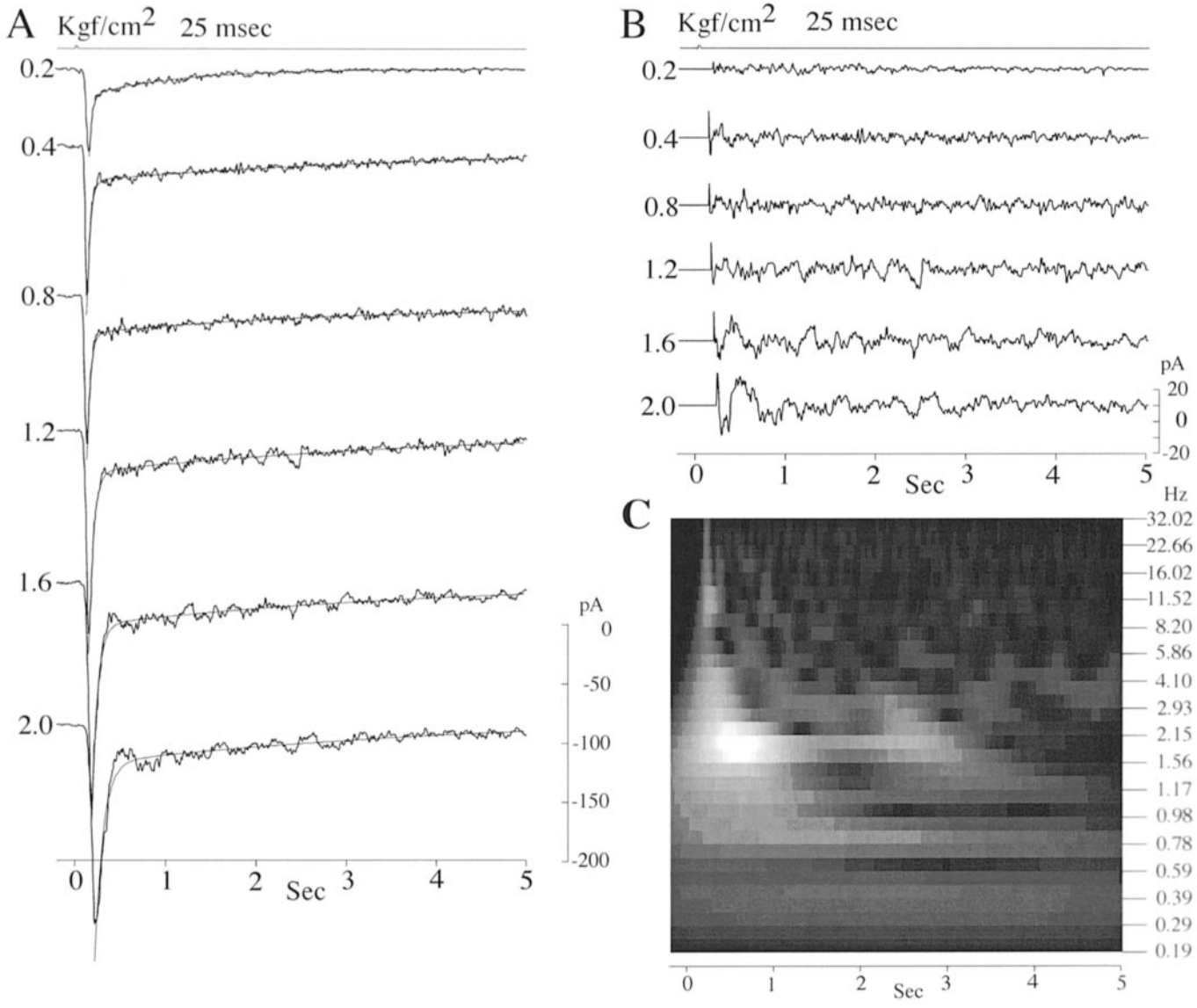

Figure 1 Oscillations of current responses of a typical cORN to the amino acid mixture. **(A)** Whole-cell inward current responses to the amino acid mixture at different stimulus ejection pressures (0.2–2.0 kgf/cm^2; duration, 25 ms) at a holding potential of –60 mV. Stimulus ejection pressure (kgf/cm^2) is shown on each trace. Top trace shows the timing of ejection pressure pulse. The decay phase of each record was fitted by a double exponential function curve. **(B)** The fitted function curve data were subtracted from the decay phase data of the record and the corresponding residue noises to the record in (A) are shown. **(C)** The power density diagram in 8 bit grayscale analyzed by the 8th-order Gabor function. The diagram was obtained from the lowest residue noises (2.0 kgf/cm^2) in (B). The dominant frequency for the record ranged between 1.56 and 2.15 Hz.

in the mean frequency between different types of ORNs [cORNs, 1.95 ± 0.25 Hz (n = 41, range 0.98–3.51); mORNs, 1.85 ± 0.22 Hz (n = 21, range 1.36–3.51); $P > 0.3$, Mann–Whitney U-test] or between different perfusion conditions [standard Ringer's solution, 1.92 ± 0.49 Hz (n = 62, range 0.98–3.15); Na-free (choline) Ringer's solution, 1.86 ± 0.28 Hz (n = 28, range 1.36–2.93); $P > 0.5$, Mann–Whitney U-test], but there was a statistical difference in the mean frequency between different holding potentials [–60 mV, 1.91 ± 0.25 Hz (n = 71, range 0.98–3.51); +20 mV, 1.59 ± 0.15 Hz (n = 13, range 1.36–2.58); $P < 0.01$, Mann–Whitney U-test].

Simulation of whole-cell current responses

As described in Materials and methods, the simulation programs were developed on the basis of a cAMP transduction model for current responses of ORNs, where it was assumed that the sum of concentrations of active CNG and CAC channels was linearly related to the whole-cell inward current response (Figure 3). The solutions for 12 differential equations using 44 different parameters (see Appendix) were calculated by the Euler or 4th-order Runge–Kutta integration methods at 1 ms integration time step. No obvious differences in the solutions obtained by these two methods were observed at 1 ms step integration. Figure 4 shows one

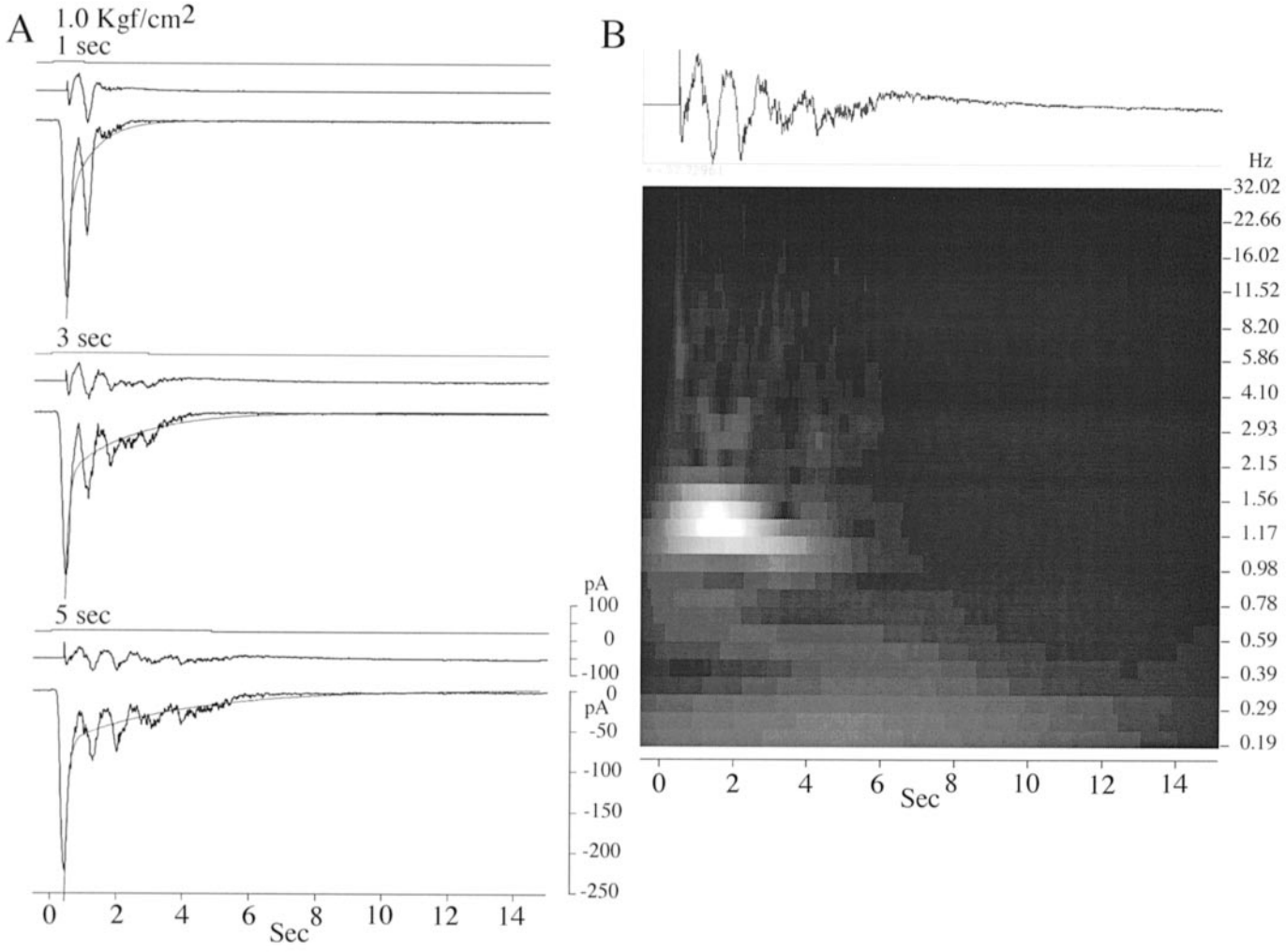

Figure 2 Oscillations of current responses of a typical mORN to the amino acid mixture. **(A)** Whole-cell inward current responses to the amino acid mixture in different stimulus durations, 1, 3 and 5 s at 1.0 kgf/cm^2 at a holding potential of –60 mV. Top trace in each record shows the timing of ejection pressure pulse. Middle trace shows the residue noises obtained by fitting of double exponential curve to the decay phase of each response record in lowest trace. **(B)** The wavelet analysis expressed by the 8 bit grayscale power density diagram using the eighth-order Gabor function. The diagram was obtained from the top residue noises, the same as that in the 5 s duration record shown in (A). The dominant frequency for the record ranged between 1.17 and 1.56 Hz.

set of solutions when the initial values of the12 functions and 44 parameters were set up as defaults for the programs shown in the Appendix. Odorant stimuli (*od*) with a 25 ms duration at different concentrations ranging from 0.01 to 10 000 μM (10^{-8} and 10^{-2} M) were applied in 20 logarithmic steps. The resulting function changes were phasic, with an initial fast rise and a slower exponential decay and return to the initial level within 6 s. For *od* concentrations >10 μM, the damped oscillations were superimposed on the decay phases of the changes. Marked oscillations occurred in five functions: the concentrations of active CNG channels (x); active CAC channels (y); active AC (v); cAMP (u); and free Ca^{2+} (q). Oscillations also occurred in the sum of concentrations of active CNG and CAC channels ($x + y$) in *od* concentrations >10 μM (Figure 4A–F), although the contribution of the concentration of active CAC channels to the sum of concentrations of ($x + y$) was small compared to the concentration of active CNG channels (note that the scale maximum in Figure 4C is one-hundredth of that in Figure 4B). Less marked oscillations were observed in concentrations of active PKA (s) and calcium–calmodulin complex (p) in *od* concentrations >10 μM (graphs not shown). The changes of all 12 functions, including the five functions with marked oscillations, became saturated in *od* concentrations >1000 μM.

Characteristics of ($x + y$) changes in the simulation

Figure 5 shows three-dimensional presentations of ($x + y$) changes, of which the polarity of y-axes was reversed to mimic actual whole-cell inward current responses. The changes in ($x + y$) increased with increased *od* concentrations and the damped oscillations were superimposed on

Table 1 Oscillation frequencies in different types of ORNs and different recording conditions

Types of ORNs/recording conditions (no. of ORNs)	Peak frequency (Hz)[a]	*P*-value[b]
1. All records		
–60 or +20 mV, standard Ringer's or Na^+-free (choline) Ringer's (41 ORNs: 31 cORNs; 10 mORNs)	1.89 ± 0.50 (92; 0.98–3.51)	–
2. Type of ORNs		
cORNs (31), –60 mV, standard Ringer's	1.95 ± 0.25 (41; 0.98–3.51)	>0.3
mORN (10), –60 mV, standard Ringer's	1.85 ± 0.22 (21; 1.36–3.51)	
3. Holding potential		
–60 mV, standard Ringer's (25 cORNs; 9 mORNs)	1.91 ± 0.25 (71; 0.98–3.51)	<0.01
+20 mV, standard Ringer's (6 cORNs)	1.59 ± 0.15 (13; 1.36–2.58)	
4. Perfusion solution		
Standard Ringer's, –60 mV (17 cORNs; 10 mORNs)	1.92 ± 0.49 (62; 0.98–3.51)	>0.5
Na^+-free (choline), –60 mV (13 cORNs)	1.86 ± 0.28 (28; 1.36–2.93)	

[a]Data of peak frequency are expressed as mean ± SD (number of observations; range)

[b]By Mann–Whitney *U*-test. Statistical significance was noted only in different holding potential conditions.

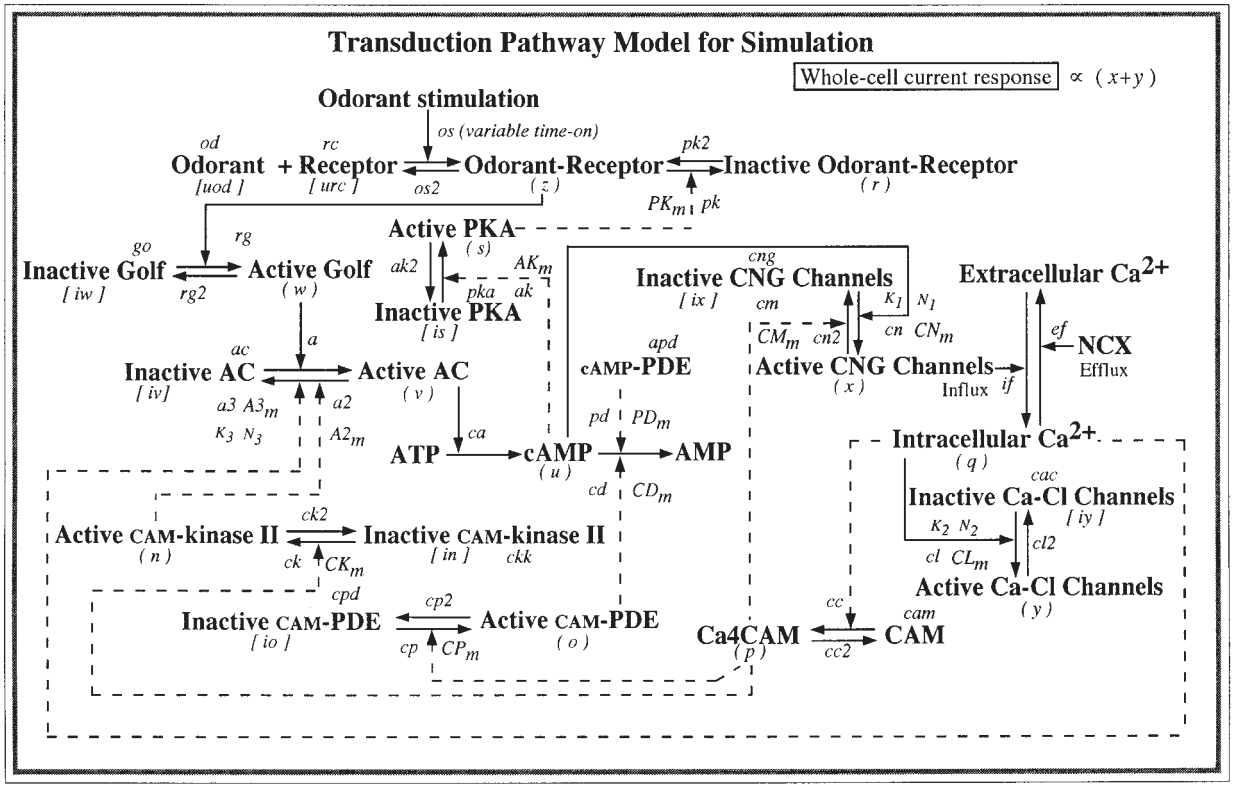

Figure 3 The cAMP transduction pathway model for the simulation. The model was constructed based on the references cited in previous work (Zufall *et al*., 1994; Nakamura, 2000). Arrows with solid lines indicate the downward regulation processes between individual enzyme reactions and arrows with dotted lines indicate the negative feedback regulation processes between them. It was assumed that the whole-cell current responses are linearly related to the sum of concentrations of active CNG and CAC channels. The definitions of character symbols in this figure and their dimensions are shown in the Appendix.

their decay phases in *od* concentrations >10 μM. The changes saturated in *od* concentrations >1000 μM. The latency for $(x + y)$ changes became shorter (from 181.8 to 22.7 ms) with increased *od* concentration. The frequency of damped oscillations increased slightly (from 0.98 to 1.39 Hz) with increased *od* concentration (Figure 5A). These characteristics of $(x + y)$ changes simulated well the odorant intensity relation of actual inward current responses shown in Figure 1.

A search for the limiting reaction components in the

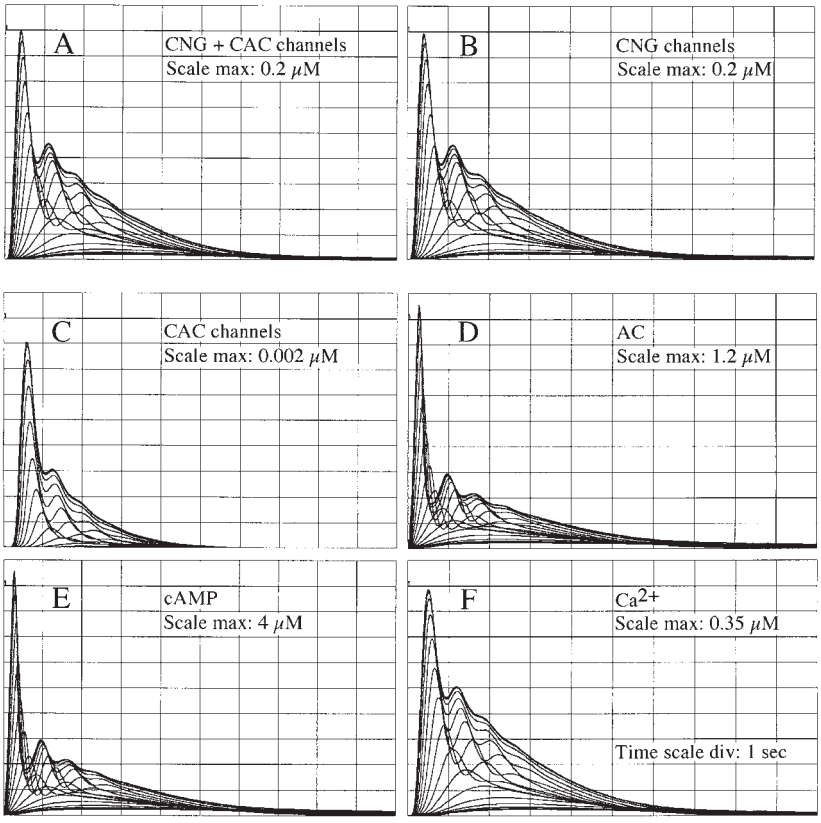

Figure 4 Oscillations in the simulation when initial values of functions and parameters were set up as a default setting for cAMP 9.2.7. Odorants were applied at 25 ms duration and at varying concentrations (0.01–10 000 μM) in 20 logarithmic steps. Marked oscillations appeared in the odorant concentration range >10 μM in five functions, concentrations of active CNG channels (*x*), active CAC channels (*y*), active AC (*v*), intracellular cAMP (*u*) and Ca^{2+} (*q*) and the sum of concentrations of *x* and *y* are shown in **(A–F)**. The stimulus mark is just visible to the left in the top grid in each part. The oscillation frequency increased with increased odorant concentration in the range between 0.98 and 1.39 Hz.

transduction model for the oscillations of $(x + y)$ changes was performed by disconnecting the feedback loops (dotted line loops in Figure 3). After many trials and errors in running the programs, direct inhibition of AC activity by Ca^{2+} was found to be only one limiting reaction for the oscillations. This is clearly shown in Figure 5B, where the maximal Ca^{2+} inhibition rate constant (*A3max*) was varied from 0 to 40 s^{-1} at 100 μM *od* stimulus with a 25 ms duration. The oscillations did not occur at 0 of *A3max*. Reaction components in the model that affected the oscillations and their frequency of $(x + y)$ were the Ca^{2+} efflux rate by NCX (*ef*) and the endogenous concentration of cAMP-PDE (*apd*). The oscillations occurred in an *ef* range >4.5 s^{-1}, where *od* stimulus was set at 100 μM and 25 ms duration. The frequency of oscillations slightly increased up to 1.62 Hz at an *ef* range of 20 s^{-1} (Figure 5C). When *apd* was set at 0 μM, there was almost no oscillation in the *od* concentration range from 0.01 to 10 000 μM (Figure 5D). On the other hand, the occurrence of oscillations of $(x + y)$ was little influenced by calmodulin-involved feedback loops. An example is shown in Figure 5E, where the endogenous concentration of calmodulin (*cam*) was changed from 1 μM as the default value to 0 μM in order to disconnect the calmodulin-involved feedback loops, calmodulin dependent phosphodiesterase (CAM-PDE) and calmodulin dependent kinase II (CAM-kinase II).

The decay speed of $(x + y)$ changes and the damping factor of the oscillations in responses to odorant stimuli >1 s long were strongly dependent on the rate constant of odorant dissociation from the receptor (*os2*) and on the endogenous concentrations of calmodulin (*cam*), CAM-PDE (*cpd*) and CAM-kinase II (*ckk*) in the calmodulin-involved feedback loops. Figure 5F shows the $(x + y)$ changes with increases of *od* concentration from 0.01 to 10 000 μM with a 3 s duration, where *os2*, *cam*, *cpd* and *ckk* were set at 20 s^{-1} and 2.2, 2.2 and 2.2 μM, respectively. Figure 5F simulates well the actual inward current responses when stimulated by odorants with durations >1 s shown in Figure 2.

Discussion

Oscillations depended on electrophysiological properties of ORNs

Oscillations superimposed on the inward current responses

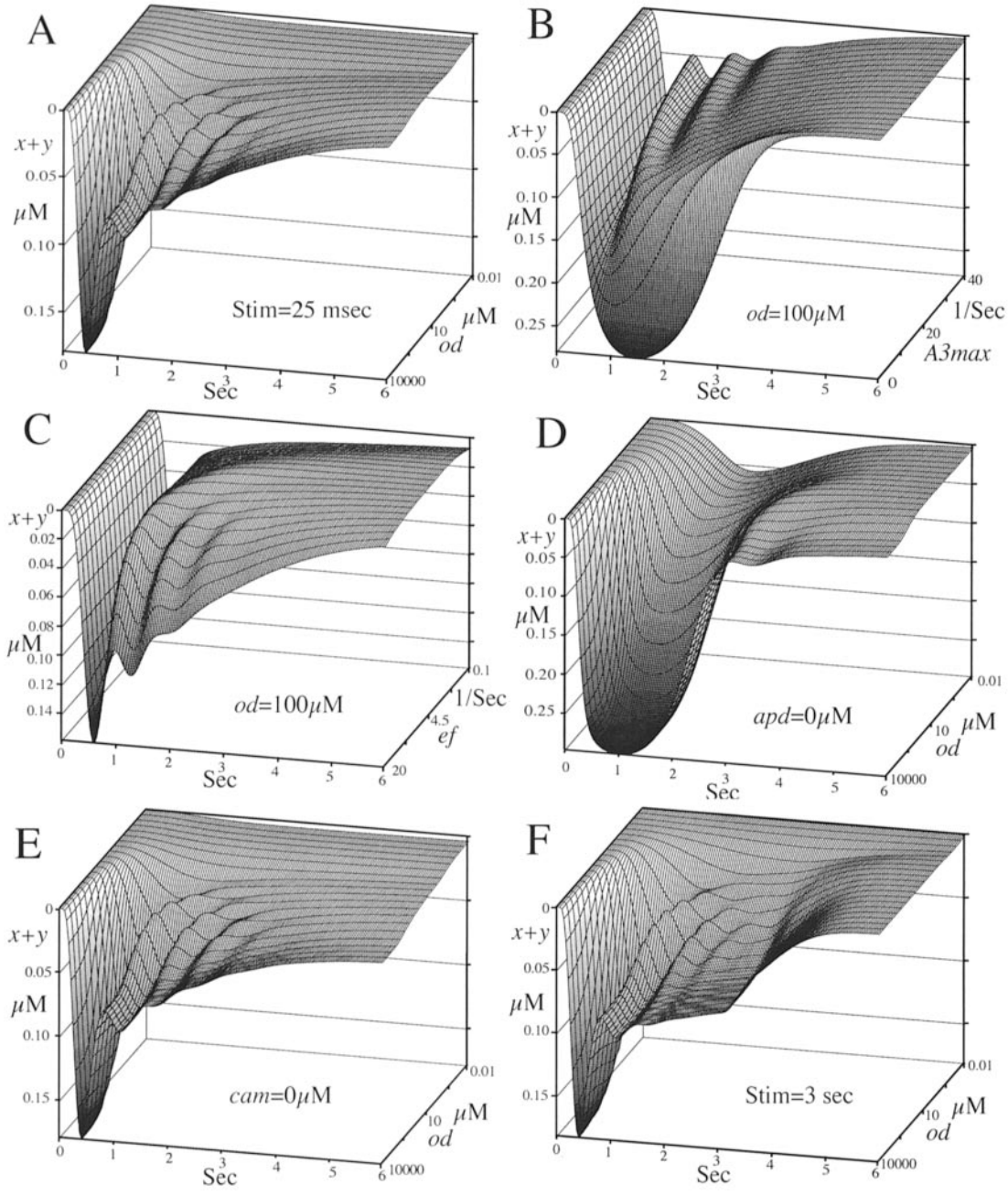

Figure 5 Three-dimensional representations of the sum of concentrations of active CNG (*x*) and CAC channels (*y*) with different parameter settings. The polarity of the *y*-axis was reversed to mimic actual whole-cell inward current responses and the polarity of the *z*-axis was reversed, except in (B), for visualization of the oscillations. Odorants of 25 ms duration and 3 s duration were applied in (A–E) and (F), respectively. Odorant concentration was changed from 0.01 to 10 000 μM in 20 logarithmic steps in (A) and (D–F) and was fixed at 100 μM in (C) and (D). **(A)** Odorant concentration dependence of ($x + y$) at the default settings of the parameters. This graph was three-dimensionally plotted from the data of the graph shown in Figure 4A. Note that the latency of the ($x + y$) changes became shorter with increases in odorant concentration, as is similarly shown in (D–F). The figure simulates well the actual whole-cell inward current responses shown in Figure 1. **(B)** The maximal rate constant of AC inactivation by Ca^{2+} (*A3max*) was stepped up from 0 to 40 s^{-1} in 20 linear steps. There were no oscillations at 0 s^{-1} of *A3max*, at which the process for direct AC inactivation by Ca^{2+} was disconnected, indicating that the process is necessary for the oscillations. **(C)** The rate constant of Ca^{2+} efflux (*ef*) was changed from 0.1 to 20 s^{-1} in 20 logarithmic steps. The oscillations appeared in the range >4.5 s^{-1}. **(D)** Odorant concentration dependence of ($x + y$) when the endogenous concentration of cAMP-PDE (*apd*) was set at 0 μM. Oscillations disappeared almost completely. **(E)** Odorant concentration dependence of ($x + y$) when the endogenous concentration of calmodulin (*cam*) was set at 0 μM to disconnect the calmodulin-involved feedback loops. Oscillatory behaviors of ($x + y$) did not change significantly. **(F)** Odorant concentration dependence of ($x + y$) changes for odorants associated with longer stimulus duration. The rate constant of odorant dissociation from odorant receptor (*os2*) was set at 20 $\mu M^{-1}s^{-1}$. The endogenous concentrations of *cam*, calmodulin-dependent phosphodiesterase (*cpd*) and calmodulin-dependent kinase II (*ckk*) were also set at 2.2 μM. The oscillations appeared in the odorant concentration range >10 μM. The figure simulates well the actual whole-cell inward current responses shown in Figure 2A.

of isolated ORNs from rainbow trout occurred in both cORNs and mORNs when stimulated by amino acid odorants at high intensity. The dominant frequency of oscillations in both types of ORNs did not differ significantly. This similarity of oscillation properties was probably due to the similarity of electrophysiological properties of the *I–V* relations and reversal potentials for the amino acid odorant between both types of ORNs (Sato and Suzuki, 2000, 2001). In addition, there was no significant difference in oscillation frequency between different perfusion conditions for different ion channel current recordings, indicating that both types of ORNs have the same kinds of efferent ion channels—CNG and CAC channels—in their transduction pathways, although these two types of ORNs might have different types of odorant receptors (Sato and Suzuki, 2001). On the other hand, the oscillation frequency was significantly different in different holding potential conditions. The dominant frequency of oscillation at –60 mV was slightly higher than at +20 mV. The results were also attributed to the voltage-dependent characteristics of the current responses to amino acid odorants, in which the decay speed of the current responses was faster in negative holding potential ranges than in positive potential ranges. Thus, the oscillation frequency of whole-cell current responses depended superficially on their electrophysiological characteristics.

Comparison with previously observed oscillations

The oscillation frequency of isolated ORNs from rainbow trout in the present study (1.89 Hz) was higher than those previously found in isolated ORNs from the frog—0.10–0.12 Hz (Frings and Lindemann, 1988) and 0.083–0.28 Hz (Reisert and Matthews, 1997, 2001a)—and was in the range of those found in the mouse—0.42–2.70 Hz (Reisert and Matthews, 2001b). Differences in oscillation frequencies might be due to the different odorant stimulation methods used in various studies; we used short periods of stimulation from 25 ms to 5 s with the pressure ejection method, while other groups used a longer odorant stimulation time of 30 s or >1 min with stepping superfusion or continuous bath application methods. The different oscillation frequencies of ORNs in different species also suggest species-specific differences in reaction components in olfactory transduction pathways of ORNs (see later discussion on simulation).

Generation mechanisms of PWs

Oscillations of current responses of ORNs should directly influence both EOG responses and nerve impulse responses of the populations of ORNs in *in vivo* preparations, since EOG responses are composed of the sums of slow potential changes of ORNs in the olfactory epithelium, and nerve impulses from the populations of ORNs are direct outputs from ORNs triggered by current or voltage responses of individual ORNs. The oscillation frequency of current responses of isolated ORNs from the rainbow trout (1.89 Hz) in the present study, however, was much lower than those of the PWs of EOGs in the channel catfish (28 Hz) (Parker *et al*., 1999; 2000) and in the toad (16 Hz) (Nakazawa *et al*., 2000), and the nerve impulse responses of small populations of ORNs in the channel catfish (20–28 Hz) (Nikonov and Caprio, 2001; Nikonov *et al*., 2002). The higher frequency of oscillations in the PWs could not be explained by the simple summation of slow oscillations of individual ORNs, because spatial and temporal excitation of individual ORNs in different locations in the olfactory epithelium would elicit the PWs as a whole (Parker *et al*., 1999). If there are electrical connections between individual ORNs in the olfactory epithelium as has been suggested (Zhang *et al*., 2000), the generation mechanism of the PWs would become much more complex.

Parameter setting in the simulation

The present simulation revealed that the oscillations of current responses of ORNs are mainly due to the oscillatory properties of intracellular cAMP and Ca^{2+} concentrations. The necessary reaction component for the oscillations in the transduction model was the direct inhibition of AC activity by Ca^{2+}. High Ca^{2+} effluxes by NCX and cAMP-PDE activity were the parameters that most influenced the oscillations. The important role of NCX in Ca^{2+} efflux in the oscillations of ORNs, as suggested by Reisert and Matthews (Reisert and Matthews, 1997, 2001a,b), was consistent with the previous result that the Ca^{2+}-chelating action of trisodium citrate on the surface of olfactory epithelium triggered and enhanced the PWs (Parker *et al*., 2000).

We used 44 different parameters in the simulation, some of which were obtained from data available in previously published studies and the references therein (Zufall *et al*., 1994; Nakamura, 2000). Since many other parameters were unknown, we took arbitrary but reasonable ranges of values in ORNs, as used in previous simulation studies (Cooper *et al*., 1995; Bhalla and Iyengar, 1999). For example, endogenous concentrations of enzymes such as *pka, go, ac, ckk, apd, cam* and *cpd* were taken as 1–5 μM per ORN. The endogenous concentrations of CNG and CAC ion channels were set at 1 μM per ORN. Unknown rate constants and their maximal rates for enzyme reactions such as *AKmax*, *PKmax, rg, a, A2max, A3max, ca, PDmax, CDmax* and *CKmax* were also set at 0.1–40 s^{-1}. In addition, the rate constants for Ca^{2+} influx (*if*) through CNG channels and efflux (*ef*) by NCX were set at 20 and 10 s^{-1}, respectively. However, essentially similar simulation results were obtained in the intracellular Ca^{2+} concentration range up to 300 nM (Leinders-Zufall *et al*., 1997, 1998), even if these values were changed to the order of several thousands per second (Hilgemann, *et al*., 1991; Niggli and Lederer, 1991) when we kept the ratio of influx and efflux rates at ~2:1. Thus, these empirically chosen values, conversely, have been

shown to be appropriate for the simulation of actual current responses in the present study.

The current carried through CAC channels is thought to contribute mostly to the whole-cell current response to odorants in the newt at ~40% of total current (Kurahashi and Yau, 1993) and in the rat at ~80% of total current (Lowe and Gold, 1993). In the present simulation, however, the contribution of the concentration of active CAC channels to $(x + y)$ was as small as one-hundredth of that of the active CNG channels. This quite different feature in the simulation might be due to our parameter setting: we ignored the unit conductances of CNG and CAC channels, and the half-maximal concentration of Ca^{2+} for CAC channel openings was set at 5.0 μM (Kleene and Gesteland, 1991), which might have been rather high for the intracellular Ca^{2+} change up to 300 nM (Leinders-Zufall *et al*., 1997, 1998).

Simulation of oscillations with lower frequency induced by prolonged stimulation

The present simulation matched the oscillations of current responses of ORNs to odorants with short stimulus durations from 25 ms to 5 s and their damped oscillation frequency was in the range of 0.98–1.62 Hz. The frequency of current or voltage oscillations observed in frog ORNs—0.10–0.12 Hz (Frings and Lindemann, 1988) and 0.083–0.28 Hz (Reisert and Matthews, 1997, 2001a)—was much lower than the frequency range of the present simulation. The damping of oscillations during prolonged stimulation of up to 1 min or more was not observed in these studies. We tried to simulate such low-frequency oscillations without damping with prolonged stimulus durations of up to 60 s with the simulation program, cAMP 9.2.8, by changing parameter settings, but we could not find such oscillations, although damped oscillations with frequencies as low as 0.4 Hz were obtained when *od* concentration, *if* and *ef* were set at 0.1 μM, 1 s^{-1} and 0.1–0.5 s^{-1}, respectively. Therefore, the present simulation model might have needed some other transduction processes than cAMP-involved processes such as IP_3-involved processes (Restrepo *et al*., 1990, 1993; Lo *et al*., 1993; Schild *et al*., 1995; Lischka *et al*., 1999; Cadiou *et al*., 2000; Iida and Kashiwayanagi, 2000) and CO/cGMP-involved processes (Zufall and Leinders-Zufall, 1997). However, since the simulation completely represented the major characteristics of current responses of ORNs to odorants with short stimulus durations—odorant-intensity-dependent response, intensity-dependent latency and adaptation—the present simulation is generally applicable to current and voltage responses of ORNs equipped with the cAMP olfactory transduction pathway in other vertebrate species.

Acknowledgements

We thank Dr Yasuhiro Ishikawa (Ishikawa Medical Clinic, Saitama, Japan) for his kind guidance during the use of MEM wavelet analysis software. We also thank Dr Michio Yazawa (Division of Chemistry, Hokkaido University) for valuable comments on the construction of the cAMP transduction model and Dr Shin Tochinai (Division of Biological Science, Hokkaido University) for uploading the cAMP 9.2.7 and 9.2.8 simulation programs and the cAMP JAVA applet versions to our web site (http://bio2.sci.hokudai.ac.jp/bio/chinou1/).

References

Adrian, E.D. (1955) *Potential oscillations in the olfactory organ*. J. Physiol. (Lond.), 128, 21–22.

Adrian, E.D. (1956) *The action of the mammalian olfactory organ.* J. Laryngol. Otol., 70, 11–14.

Bhalla, U.S. and **Iyengar, R.** (1999) *Emergent properties of networks of biological signaling pathways.* Science, 283, 381–387.

Cadiou, H., Sienaert, I., Vanlingen, S., Parys, J.B., Molle, G. and **Duclohier, H.** (2000) *Basic properties of an inositol channel in carp olfactory cilia.* Eur. J. Neurosci., 12, 2805–2811.

Cooper, D.M.F., Mons, N. and **Karpen, J.W.** (1995) *Adenylyl cyclases and the interaction between calcium and cAMP signalling*. Nature, 374, 421–424.

Desmaisons, D., Vincent, J.-D. and **Lledo, P.-M.** (1999) *Control of action potential timing by intrinsic subthreshold oscillations in olfactory bulb output neurons.* J. Neurosci., 19, 10727–10737.

Dorries, K.M. and **Kauer, J.S.** (2000) *Relationships between odor-elicited oscillations in the salamander olfactory epithelium and olfactory bulb.* J. Neurophysiol., 83, 754–765.

Frings, S. and **Lindemann, B.** (1988) *Odorant response of isolated olfactory receptor cells is blocked by amiloride.* J. Membrane Biol., 105, 233–243.

Gershenfeld, N. (1999) The Nature of Mathematical Modeling. Cambridge University Press, Cambridge.

Hamilton, K.A. and **Kauer, J.S.** (1989) *Patterns of intracellular potentials in salamander mitral/tufted cells in response to odor stimulation.* J. Neurophysiol., 59, 609–625.

Hilgemann, D.W., Nicoll, D.A. and **Philipson, K.D.** (1991) *Charge movement during Na^+ translocation by native and cloned cardiac Na^+/Ca^{2+} exchanger.* Nature, 352, 715–718.

Hutcheon, B. and **Yarom, Y.** (2000) *Resonance, oscillation and the intrinsic frequency preferences of neurons.* Trends Neurosci., 23, 216–222.

Iida, A. and **Kashiwayanagi, M.** (2000) *Responses to putative second messengers and odorants in water nose olfactory neurons of* Xenopus laevis. Chem. Senses, 25, 55–59.

Ishikawa, Y. (2000) Wavelet Analysis for Clinical Medicine. Igaku-Shuppan, Tokyo (in Japanese).

Kleene, S.J. and **Gesteland, R.C.** (1991) *Calcium-activated chloride conductance in frog olfactory cilia*. J. Neurosci., 11, 3624–3629.

Kurahashi, T. and **Yau, K.-W.** (1993) *Co-existence of cationic and chloride components in odorant-induced current of vertebrate olfactory receptor cells*. Nature, 363, 71–74.

Lam, Y.-W., Cohen, L.B., Wachowiak, M. and **Zochowski, M.R.** (2000) *Odors elicit three different oscillations in the turtle olfactory bulb*. J. Neurosci., 20, 749–762.

Leinders-Zufall, T., Rand, M.N., Shepherd, G.M., Greer, C.A. and **Zufall, F.** (1997) *Calcium entry through cyclic nucleotide-gated channels in individual cilia of olfactory receptor cells: spaciotemporal dynamics.* J. Neurosci., 17, 4136–4148.

Leinders-Zufall, T., Greer, C.A., Shepherd, G.M. and **Zufall, F.** (1998) *Imaging odor-induced calcium transients in single olfactory cilia: specificity of activation and role in transduction.* J. Neurosci., 18, 5630–5639.

Lischka, F.W., Zviman, M.M., Teeter, J.H. and **Restrepo, D.** (1999) *Characterization of inositol-1,4,5-trisphosphate-gated channels in the plasma membrane of rat olfactory neurons.* Biophys. J., 76, 1410–1422.

Lo Y. H., Bradley, T.M. and **Rhoads, D.E.** (1993) *Stimulation of Ca^{2+}-regulated olfactory phospholipase C by amino acids*. Biochemistry, 32, 12358–12362.

Lowe, G. and **Gold, G.H.** (1993) *Nonlinear amplification by calcium-dependent chloride channels in olfactory receptor cells.* Nature, 366, 283–286.

Mallat, S. (1999) A Wavelet Tour of Signal Processing, 2nd edn. Academic Press, London.

Mathews, D.F. (1972) *Response patterns of single units in the olfactory bulb of the rat to odor.* Brain Res., 47, 389–400.

Nakamura, T. (2000) *Cellular and molecular constituents of olfactory sensation in vertebrates.* Comp. Biochem. Physiol., A126, 17–32.

Nakazawa, H., Kaji, S. and **Ishii, S.** (2000) *Oscillatory electric potential on the olfactory epithelium observed during the breeding migration period in the Japanese toad,* Bufo japonicus*.* Zool. Sci., 17, 293–300.

Niggli, E. and **Lederer, W.J.** (1991) *Molecular operations of the sodium–calcium exchanger revealed by conformation currents.* Nature, 349, 621–624.

Nikonov, A.A. and **Caprio, J.** (2001) *Electrophysiological evidence for a chemotopy of biologically relevant odors in the olfactory bulb of the channel catfish.* J. Neurophysiol., 86, 1869–1876.

Nikonov, A.A., Parker, J.M. and **Caprio, J.** (2002) *Odorant-induced olfactory receptor neural oscillations and their modulation of olfactory bulbar responses in the channel catfish.* J. Neurosci., 22, 2352–2362.

Ottoson, D. (1956) *Analysis of the electrical activity of the olfactory epithelium*. Acta Physiol. Scand., 35, 1–83.

Ottoson, D. (1959a) *Comparison of slow potentials evoked in the frog's nasal mucosa and olfactory bulb by natural stimulation.* Acta Physiol. Scand., 47, 149–159.

Ottoson, D. (1959b) *Studies on slow potentials in the rabbit's olfactory bulb and nasal mucosa*. Acta Physiol. Scand., 47, 136–148.

Parker, J.M., Lindemann, B. and **Caprio, J.** (1999) *Electrical communication among olfactory receptor neurons by peripheral waves.* Chem. Senses, 24, 576.

Parker, J.M., Chang, Q. and **Caprio, J.** (2000) *Citrate enhances olfactory receptor responses and triggers oscillatory receptor activity in the channel catfish.* J. Neurophysiol., 83, 2676–2681.

Reisert, J. and **Matthews, H.R.** (1997) *Effects of sodium removal on the oscillatory response to prolonged stimulation in frog olfactory receptor cells.* J. Physiol. (Lond.), 499, 88P.

Reisert, J. and **Matthews, H.R.** (2001a) *Response properties of isolated mouse olfactory receptor cells.* J. Physiol. (Lond.), 530, 113–122.

Reisert, J. and **Matthews, H.R.** (2001b) *Responses to prolonged odour stimulation in frog olfactory receptor cells.* J. Physiol. (Lond.), 534, 179–191.

Restrepo, D., Miyamoto, T., Bryant, B.P. and **Teeter, J.H.** (1990) *Odor stimuli trigger influx of calcium into olfactory neurons of the channel catfish.* Science, 249, 1166–1168.

Restrepo, D, Boekhoff, I. and **Breer, H.** (1993) *Rapid kinetic measurement of second messenger formation in olfactory cilia from channel catfish.* Am. J. Physiol., 264, C906–C911.

Sato, K. and **Suzuki, N.** (2000) *The contribution of a Ca^{2+}-activated Cl^- conductance to amino-acid-induced inward current responses of ciliated olfactory neurons of the rainbow trout.* J. Exp. Biol., 203, 253–262.

Sato, K. and **Suzuki, N.** (2001) *Whole-cell response characteristics of ciliated and microvillous olfactory receptor neurons to amino acids, pheromone candidates and urine in rainbow trout.* Chem. Senses, 26, 1145–1156.

Schild, D., Lischka, F.W. and **Restrepo, D.** (1995) *$InsP_3$ causes an increase in apical $[Ca^{2+}]_i$ by activating two distinct current components in vertebrate olfactory receptor cells.* J. Neurophysiol., 73, 862–866.

Schutter, E. de (2001) Computational Neuroscience: Realistic Modeling for Experimentalists. CRC Press, Boca Raton, FL.

Shibuya, T. and **Tucker, D.** (1967) *Single unit responses of olfactory receptors in vultures.* In Hayashi, T. (ed.), Olfaction and Taste II. Pergamon Press, New York, pp. 219–233.

Sutterlin, A.M. and **Sutterlin, N.** (1971) *Electrical responses of the olfactory epithelium of Atlantic salmon (*Salmo salar*).* J. Fish. Res. Bd Canada, 28, 565–572.

Takagi, S.F. and **Shibuya, T.** (1960a) *Potential oscillations in the lower olfactory pathway of the toad.* Nature, 186, 724.

Takagi, S.F. and **Shibuya, T.** (1960b) *The potential oscillations observed in the olfactory epithelium, nerve and bulb to the toad and frog.* Jpn. J. Physiol., 10, 499–508.

Takagi, S.F. and **Shibuya, T.** (1961) *Studies on the potential oscillation appearing in the olfactory epithelium of the toad*. Jpn. J. Physiol., 11, 23–27.

Tucker, D. (1975a) *The role of respiratory ventilation in reliably obtaining electrical waves from olfactory mucosa and nerve in response to odorous stimulation.* In Ichioka, M. (ed.), Proceedings of the 9th Japanese Symposium on Olfaction and Taste, Osaka (Tokyo), pp. 16–17.

Tucker, D. (1975b) *Waves elicited from peripheral neural tissue (olfactory) in response to odorous stimulation.* Biophys. J., 15, 271a.

Tucker, D. and **Suzuki, N.** (1972) *Olfactory responses to Schreckstoff of catfish*. In Schneider, D. (ed.), Olfaction and Taste IV. Wissenschaftliche Verlagsgesellschaft, Stuttgart, pp. 121–127.

Zhang C., Finger, T.E. and **Restrepo, D.** (2000) *Mature olfactory receptor neurons express connexin 43.* J. Comp. Neurol., 426, 1–12.

Zufall, F. and **Leinders-Zufall, T.** (1997) *Identification of a long-lasting form of odor adaptation that depends on the carbon monoxide/cGMP second-messenger system.* J. Neurosci., 17, 2703–2712.

Zufall, F., Firestein, S. and **Shepherd, G.M.** (1994) *Cyclic nucleotide-gated ion channels and sensory transduction in olfactory receptor neurons.* Annu. Rev. Biophys. Biomol. Struct., 23, 577–607.

Accepted August 7, 2002

Appendix

Differential equations

$$dx/dt = cn*ix - cn2*x - cm*x$$

$$dy/dt = cl*iy - cl2*y$$

$$dz/dt = urc*os*uod - os2*z - pk*z + pk2*r$$

$$dw/dt = rg*iw*z - rg2*w$$

$$dv/dt = iv*a*w - a3*v - a2*v$$

$$du/dt = ca*v - pd*u - cd*u$$

$$ds/dt = is*ak - ak2*s$$

$$dr/dt = pk*z - pk2*r$$

$$dq/dt = if*x - ef*q$$

$$dp/dt = cc*cam*(q/4) - cc2*p$$

$$do/dt = cp*io - cp2*o$$

$$dn/dt = ck*in - ck2*n$$

where

$$io = cpd - o$$

$$in = ckk - n$$

$$iv = ac - v$$

$$ix = cng - x$$

$$iy = cac - y$$

$$iw = go - w$$

$$urc = rc - z - r$$

$$uod = od - z - r$$

$$is = pka - s$$

$$cd = CDmax*o$$

$$cp = CPmax*p$$

$$ck = CKmax*p$$

$$cm = CMmax*p$$

$$a2 = A2max*n$$

$$pk = PKmax*s$$

$$ak = AKmax*u$$

$$pd = PDmax*apd$$

$$cn = CNmax*u\text{^}N1/(u\text{^}N1 + K1\text{^}N1)$$

$$cl = CLmax*q\text{^}N2/(q\text{^}N2 + K2\text{^}N2)$$

$$a3 = A3max*q\text{^}N3/(q\text{^}N3 + K3\text{^}N3)$$

Definition of functions and parameters, and default settings of these values for numerical calculation

x: concentration of active CNG channels (μM) = 0.0001 (*x*0)
y: concentration of active Ca–Cl channels (μM) = 0.0001 (*y*0)
z: concentration of odorant–receptor complex (μM) = 0.001 (*z*0)
w: concentration of active Golf (μM) = 0.001 (*w*0)
v: concentration of active AC (μM) = 0.001 (*v*0)
u: concentration of cAMP (μM) = 0.001 (*u*0)
s: concentration of active PKA (μM) = 0.001 (*s*0)
r: concentration of inactive odorant–receptor complex (μM) = 0.001 (*r*0)
q: concentration of intracellular calcium ions (μM) = 0.001 (*q*0)
p: concentration of Ca4CAM (μM) = 0.001 (*p*0)
o: concentration of active CAM-PDE (μM) = 0.001 (*o*0)
n: concentration of active CAM-kinase II (μM) = 0.001 (*n*0)

od: concentration of odorants (μM) = 1.0
uod: concentration of unbound odorants (μM)
rc: concentration of receptor (μM) = 1.0
urc: concentration of unbound receptor (μM)
os: rate of odorant binding to receptor (1/μMs) = 0.1
os2: rate of odorant dissociation from receptor (1/s) = 2.0
pka: concentration of PKA (μM) = 1.0
is: concentration of inactive PKA (μM)
ak: rate of PKA activation by cAMP (1/s)
AKmax: maximal rate of PKA activation by cAMP (1/μMs) = 0.1
ak2: rate of PKA inactivation (1/s) = 1.0
pk: rate of receptor inactivation by active PKA (1/s)
PKmax: maximal rate of receptor inactivation by active PKA (1/μMs) = 1.0
pk2: rate of reversal of receptor inactivation (1/s) = 0.1
go: concentration of Golf (μM) = 1.0
iw: concentration of inactive Golf (μM)
rg: rate of activation of Golf by odorant–receptor complex (1/μMs) = 10
rg2: rate of inactivation of Golf (1/s) = 2.0
ac: concentration of AC (μM) = 5.0
iv: concentration of inactive AC (μM)
a: rate of AC activation by active Golf (1/μMs) = 2.0
ckk: concentration of CAM-kinase II (μM) = 1.0
in: concentration of inactive CAM-kinase II (μM)
a2: rate of AC inactivation by CAM-kinase II (1/s)
A2max: maximal rate of AC inactivation by CAM-kinase II (1/μMs) = 1 0
a3: rate of AC inactivation by calcium ions (1/s)
A3max: maximal rate of AC inactivation by calcium ions (1/s) = 40
ca: rate of cAMP synthesis by active AC (1/s) = 40
apd: concentration of cAMP-PDE (μM) = 1.0
pd: rate of cAMP hydrolysis by cAMP-PDE (1/s)
PDmax: maximal rate of cAMP hydrolysis by cAMP-PDE (1/μMs) = 10
cng: concentration of CNG channels (μM) = 1.0

ix: concentration of inactive CNG channels (μM)
cn: rate of CNG channel activation by cAMP (1/s)
CNmax: maximal rate of CNG channel activation by cAMP (1/s) = 5.0
cn2: rate of CNG channel inactivation (1/s) = 10
cam: concentration of CAM (μM) = 1.0
cc: rate of calcium binding to CAM (1/μMs) = 0.1
cc2: rate of calcium dissociation from CAM (1/s) = 1.0
cm: rate of CNG channel inactivation by Ca4CAM (1/s)
CMmax: maximal rate of CNG channel inactivation by Ca4-CAM (1/μMs) = 10
if: rate of calcium ion influx through CNG channels (1/s) = 20
ef: rate of calcium ion efflux by NCX (1/s) = 10
cac: concentration of Ca–Cl channels (μM) = 1.0
iy: concentration of inactive Ca–Cl channels (μM)
cl: rate of Ca–Cl channel activation by calcium ions (1/s)
CLmax: maximal rate of Ca–Cl channel activation by calcium ions (1/s) = 5.0
cl2: rate of Ca–Cl channel inactivation (1/s) = 10
cpd: concentration of CAM-PDE (μM) = 1.0
io: concentration of inactive CAM-PDE (μM)
cp: rate of CAM-PDE activation by Ca4CAM (1/s)
CPmax: maximal rate of CAM-PDE activation by Ca4CAM (1/μMs) = 10
cp2: rate of CAM-PDE inactivation (1/s) = 0.01
cd: rate of cAMP hydrolysis by CAM-PDE (1/s)
CDmax: maximal rate of cAMP hydrolysis by CAM-PDE (1/μMs) = 20
ck: rate of CAM-kinase II activation by Ca4CAM (1/s)
CKmax: maximal rate of CAM-kinase II activation by Ca4CAM (1/μMs) = 10
ck2: rate of CAM-kinase II inactivation (1/s) = 0.01
K1: concentration of cAMP at which CNG channel activation is half-maximal (μM) = 3.4
K2: concentration of calcium ions at which Ca–Cl channel activation is half-maximal (μM) = 5.0
K3: concentration of calcium ions at which AC inhibition is half-maximal (μM) = 0.2
N1,*2*,*3*: Hill coefficients for the processes = 1.4, 2 and 3